Scientia Iranica D (2018) 25(3), 1507–1522

SCIENTIA IRANICA

Sharif University of Technology

Scientia Iranica

Transactions D: Computer Science & Engineering and Electrical Engineering

http://scientiairanica.sharif.edu

Sliding-mode control for a DFIG-based wind-power generation system with series grid-side converter under unbalanced grid voltage conditions

S. Abazari* and S. Farajzadeh Dehkordi

Department of Electrical Engineering, University of Shahrekord, Shahrekord, P.O. Box 115, Iran.

Received 2 October 2015; received in revised form 30 July 2016; accepted 3 October 2016

KEYWORDS

Doubly Fed Induction Generator (DFIG);
Unbalanced grid voltage;
Rotor-Side Converter (RSC);
Grid-Side Converter (GSC);
Series Grid-Side Converter (SGSC);
Sliding-Mode Control (SMC).

Abstract. In this paper, the power quality in a wind power generation system is studied. It is shown that adding a Series Grid-Side Converter (SGSC) to the Doubly Fed Induction Generator (DFIG) structure and applying a suitable control algorithm will make the system able to compensate for the adverse effects of the voltage unbalance and, consequently, it can improve the power quality. In order to decrease design complexity and implement the control algorithms in the stationary reference frame, a Sliding-Mode Control (SMC) method for controlling the DFIG system with SGSC is proposed. One of the advantages of the proposed method in this paper is its robustness to parameter variations both in the DFIG and the connected network. Moreover, the designed controller leads to a fast dynamic response. It should be mentioned that a coordinated control is carried out between SGSC and the other DFIG converters. The simulation results approve the validity of the mentioned advantages and the effectiveness of the proposed method.

1. Introduction

Nowadays, there is a high demand for the electrical energy. This kind of energy is traditionally generated in electrical power plants, which use fossil fuel sources or natural gas. However, a limited amount of the above energy sources for power plants can be found in nature. Moreover, the prices of these sources increase rapidly. More importantly, these sources are not environmentally friendly. Therefore, the need to generate clean electrical energy has been one of the most challenging engineering problems in recent years. Among different renewable energy sources, the need for the wind energy is growing fast. In modern wind power generation systems, one of the generators extended and frequently employed is the Doubly Fed Induction Generator (DFIG).

The DFIG structure is based on applying 2 different converters. The first converter is the Grid-Side Converter (GSC) and the other one is the Rotor-Side Converter (RSC). Wind farms are mainly located in rural areas where nonlinear, asymmetric loads, and grid faults can lead to frequent disturbances [1-3]. As a consequence, unbalanced and harmonic disturbances are inevitable in the wind power systems. If DFIG is not controlled by unbalanced voltage, it may cause oscillations with double frequency in electromagnetic torque, active and reactive powers injected to the grid, and mechanical components fatigue [4]. Different methods have been introduced to control the DFIG structure. In some results, the conventional control scheme of grid-connected DFIGs is generally based on vector

*. *Corresponding author. Fax: +98 38 32324438*
E-mail addresses: abazari-s@eng.sku.ac.ir (S. Abazari); sajadfarajzadeh2014@gmail.com (S. Farajzadeh Dehkordi)

doi: 10.24200/sci.2017.4367

control with Stator Voltage Orientation (SVO) [5,6] or Stator Flux Orientation (SFO) [7,8]. The main drawback of these methods is the burden of adjusting PI parameter. In addition, these control methods are not robust against parameters variations. In [9], a dual PI controller has been employed for adjusting both positive and negative components from rotor current. In [10], an auxiliary PI controller has been added to the dual PI one to adjust rotor compensator current. A proportional-integral-resonance controller is used in order to prevent positive and negative sequences extractions from rotor current [11,12]. Direct Torque Control (DTC) technique, which is robust against changes in machine parameters, has been used for induction machine [13,14]. Similar to DTC, Direct Power Control (DPC) has been used for controlling wind power generation systems based on DFIG [15-18]. However, applying these methods leads to variable switching frequency, large electromagnetic torque, and output power ripple due to hysteresis blocks, see [13-18]. Besides, the complexity of designing in these methods increases. In [18-20], Sliding-Mode Control (SMC) method has been introduced for DFIG control because of its easy implementation and robustness. SMC has recently been introduced for DFIG control connected to the ideal grid voltage because of its easy implementation and robustness [21-24]. In [25-27], SMC has been used to cancel the fluctuation in the electromagnetic torque and output power, but the final performances of applying these control methods are not still satisfactory. It seems that it is not possible to cancel the relatively large stator and rotor current unbalances, electromagnetic torque, and power pulsations simultaneously in the DFIG by using only 2 converters because of the negative-sequence voltage. Therefore, a new DFIG configuration with an additional grid-side converter in series with the generator's stator windings is proposed in order to eliminate the negative-sequence voltage and its adverse effects on the DFIG, see [28-30]. In these results, the proposed method for controlling the SGSC is to apply a PI control law. However, the complexity of adjusting the PI controller coefficients still remains. In [31], the PI plus resonant ($PI + R$) controllers are used for the SGSC voltage control (tuning) and PGSC current control (tuning), respectively, under harmonically distorted voltage conditions in the rotating positive $(dq)^+$ reference frame.

This method avoids sequential decomposition of currents and voltages, which in turn avoids the slight errors caused by the decomposition procedure. However, this solution is not robust against parameter variations, because the nonlinear cross-coupling between the direct and the quadrature components is compensated for by the feed forward terms, which are dependent on the parameters of DFIG, SGSC, and grid.

In this paper, by applying a suitable SMC control law for a DFIG system with SGSC, the inherent complexity of designing of the controller is removed. Moreover, this control law is robust against the parameter variations in the system. More importantly, a coordinated control is carried out among the 3 converters.

This paper is organized as follows: in Section 2, the DFIG plus SGSC configuration is introduced. Section 3 is devoted to the modeling of SGSC and application of the SMC law to the above system. In Sections 4 and 5, an SMC for both RSC and GSC is proposed. Section 6 represents the schematics of the control system in the DFIG system with SGSC. In Section 7, a simulation is provided, which shows effectiveness of the obtained results in this paper. The robustness properties of the proposed control law together with the response of the system are examined under the unbalanced voltage conditions. Section 8 is the conclusion of the paper.

2. Configuration of a DFIG system with SGSC

Figure 1 shows a DFIG system accompanied by the SGSC. In this structure, SGSC is in series with the network and the DFIG stator-side through three winding transformers. The DC-link is shared among GSC, RSC, and SGSC.

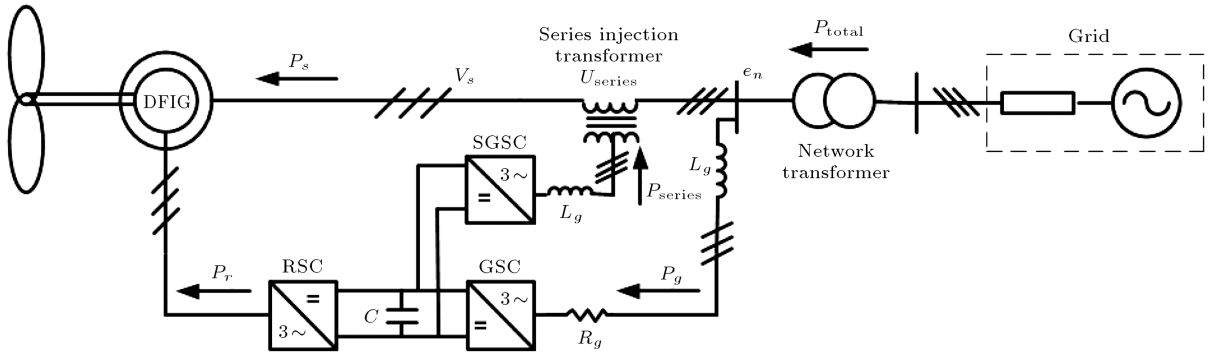

Figure 1. A DFIG system accompanied by SGSC.

With proper injection of voltage by SGSC, the voltage of the stator can be suitably controlled. According to the figure, the voltage of the stator can be written as:

$$V_s = e_n - U_{\text{series}}, \tag{1}$$

where e_n is the grid voltage, U_{series} is the injected voltage by the third converter, and V_s is the stator voltage. In the following, the DFIG structure, as shown in Figure 1, in the unbalanced voltage criteria will be investigated and modeled.

3. Behaviors of the DFIG system with SGSC during grid voltage unbalance

Under unbalanced grid voltage, the grid voltage with respect to the stationary reference frame can be expressed as [32]:

$$e_{\alpha\beta n} = e_{\alpha\beta n+} + e_{\alpha\beta n-} \tag{2}$$

In order to balance the stator voltage, the negative sequence of grid voltage and voltage drop on the impedance of the series transformer due to the positive sequence can be compensated for by using SGSC. This compensation also keeps the DFIG stator voltage in line with the positive-sequence grid voltage. Hence, the series injected voltage of SGSC can be expressed as:

$$U_{\text{series}\alpha\beta} = e_{\alpha\beta n-} - U_{\text{com}+}, \tag{3}$$

where $e_{\alpha\beta n-}$ is the negative sequence grid voltage caused by the unbalanced voltage and $U_{\text{com}+}$ is the error of the positive sequence voltage due to the voltage drop on the impedance of the series transformer, which needs to be compensated for. In the next subsection, the modeling of the SGSC with respect to its structure will be discussed.

3.1. Modeling of SGSC

The structure of SGSC is shown in Figure 2. The electrical equations describing the behavior of SGSC referred to as the stationary reference frame are:

$$U_{sg\alpha\beta n} = R_g i_{s\alpha\beta} + L_g \frac{di_{s\alpha\beta}}{dt} - U_{\text{series}\alpha\beta}, \tag{4}$$

$$P_{\text{series}} = \frac{3}{2}(U_{\text{series}\alpha} i_{s\alpha} + U_{\text{series}\beta} i_{s\beta}), \tag{5}$$

$$Q_{\text{series}} = \frac{3}{2}(U_{\text{series}\beta} i_{s\alpha} - U_{\text{series}\alpha} i_{s\beta}), \tag{6}$$

where $U_{sg\alpha\beta n}$ is the space vector relating to the voltage between the middle points of the converter legs and the node n in the stationary reference frame. U_{sgaN}, U_{sgbN}, and U_{sgbN} are the voltages between the middle points of the converter legs and the node N.

The relationship between $U_{sg\alpha n}$, $U_{sg\beta n}$, and the voltage signals U_{sgaN}, U_{sgaN}, and U_{sgcN} represented in Figure 2 is:

$$\begin{cases} \begin{bmatrix} U_{sg\alpha n} \\ U_{sg\beta n} \end{bmatrix} = M_2 M_1 \begin{bmatrix} U_{sgaN} \\ U_{sgbN} \\ U_{sgcN} \end{bmatrix} \\ U_{sg\alpha\beta n} \equiv M_2 M_1 U_{sgN} \end{cases} \tag{7}$$

where:

$$\begin{cases} U_{sg\alpha\beta n} = \begin{bmatrix} U_{sg\alpha n} & U_{sg\beta n} \end{bmatrix}^T \\ U_{sgN} = \begin{bmatrix} U_{sgaN} & U_{sgbN} & U_{sgcN} \end{bmatrix}^T \end{cases} \tag{8}$$

$$\begin{cases} M_1 = \dfrac{1}{3} \begin{bmatrix} 2 & -1 & -1 \\ -1 & 2 & -1 \\ -1 & -1 & 2 \end{bmatrix} \\ M_2 = \dfrac{2}{3} \begin{bmatrix} 1 & -0.5 & -0.5 \\ 0 & \frac{\sqrt{3}}{2} & -\frac{\sqrt{3}}{2} \end{bmatrix} \end{cases} \tag{9}$$

and M_1 is the transformation matrix between $U_{sg\alpha\beta n}$ and U_{sgN} and M_2 is the Clarke's transformation Matrix. Beneficially, no zero sequence term appears in the expression of this Clarke's transformation. In the next subsection, the control algorithm is designed for the SGSC.

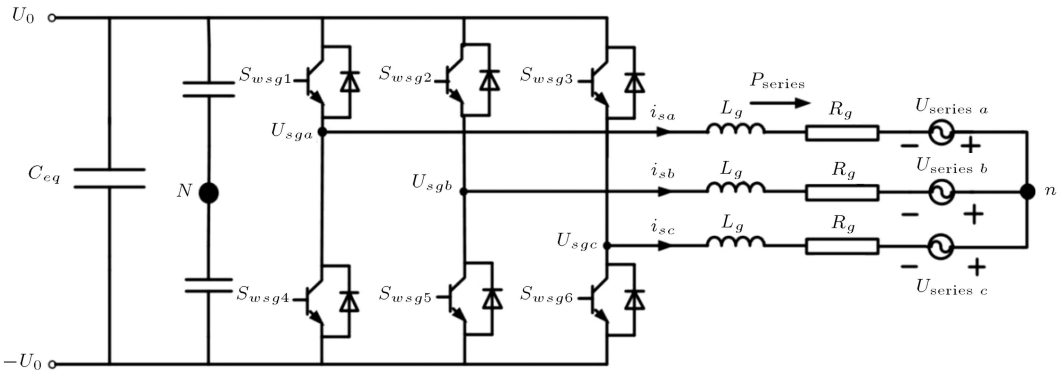

Figure 2. Structure of the SGSC.

3.2. Applying the SMC for SGSC

As it is stated, the injected series voltage of SGSC (U_{series}) must be adjusted in such a way that the stator voltage DFIG becomes balanced to keep the DFIG stator voltage in line with the positive-sequence grid voltage. Considering Eq. (4), without taking time derivative of the switching variables into account, the control inputs will be achieved and the relative degree of the system becomes 0. Thus, the order of the SMC to be designed must be at least equal to the relative degree of the system. As a result, the sliding surfaces or switching variables are designed as:

$$\begin{cases} S_{U\text{series}\alpha} = \int e_{U\text{series}\alpha}\, dt \\ S_{U\text{series}\beta} = \int e_{U\text{series}\beta}\, dt \end{cases} \tag{10}$$

where:

$$\begin{cases} e_{U\text{series}\alpha} = U^*_{\text{series}\alpha} - U_{\text{series}\alpha} \\ e_{U\text{series}\beta} = U^*_{\text{series}\beta} - U_{\text{series}\beta} \end{cases} \tag{11}$$

$U^*_{\text{series}\alpha}$ and $U^*_{\text{series}\beta}$ are the injected reference series voltage values by SGSC, which can be extracted from Eq. (3). The dynamics of the switching variables can be derived from Eq. (10) as:

$$\begin{cases} \dot{S}_{U\text{series}\alpha} = e_{U\text{series}\alpha} \\ \dot{S}_{U\text{series}\beta} = e_{U\text{series}\beta} \end{cases} \tag{12}$$

By substituting Eqs. (4) and (11) into Eq. (12), the result will be:

$$\begin{cases} \begin{bmatrix} \dot{S}_{U\text{series}\alpha} \\ \dot{S}_{U\text{series}\beta} \end{bmatrix} = \begin{bmatrix} F_{U\text{series}\alpha} \\ F_{U\text{series}\beta} \end{bmatrix} - \begin{bmatrix} -1 & 0 \\ 0 & -1 \end{bmatrix} \begin{bmatrix} U_{sg\alpha n} \\ U_{sg\beta n} \end{bmatrix} \\ \dot{S}_{U\text{series}\alpha\beta} \equiv F_{U\text{series}\alpha\beta} - JU_{\text{series}\alpha\beta} \end{cases} \tag{13}$$

where:

$$\begin{cases} \dot{S}_{U\text{series}\alpha\beta} = \begin{bmatrix} \dot{S}_{U\text{series}\alpha} & \dot{S}_{U\text{series}\beta} \end{bmatrix}^T \\ F_{U\text{series}\alpha\beta} = \begin{bmatrix} F_{U\text{series}\alpha} & F_{U\text{series}\beta} \end{bmatrix}^T \\ J = \begin{bmatrix} -1 & 0 \\ 0 & -1 \end{bmatrix} \end{cases} \tag{14}$$

and:

$$\begin{cases} F_{U\text{series}\alpha} = h_1(U^*_{\text{series}\alpha}, i_{\alpha s}, v_{\alpha s}) \\ F_{U\text{series}\beta} = h_2(U^*_{\text{series}\beta}, i_{\beta s}, v_{\beta s}) \end{cases} \tag{15}$$

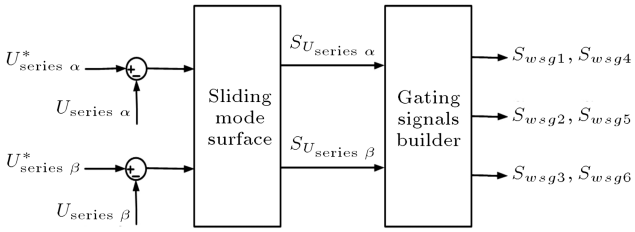

Figure 3. Control scheme of series grid-side power converter.

h_1 and h_2 are functions of the state variables. Regarding the sliding-mode control method [33], the control inputs are:

$$\{U_{sgN} = u_0 \text{sgn}(S_{sgabc}), \tag{16}$$

where $S_{sgabc} = \begin{bmatrix} S_{sga} & S_{sgb} & S_{sgc} \end{bmatrix}^T$. Finally, by replacing Eqs. (7) and (16) in Eq. (13), we have:

$$\begin{cases} \dot{S}_{U\text{series}\alpha\beta} = F_{U\text{series}\alpha\beta} - JM_2M_1 \begin{bmatrix} u_0\text{sgn}(S_{sga}) \\ u_0\text{sgn}(S_{sgb}) \\ u_0\text{sgn}(S_{sgc}) \end{bmatrix} \\ E \equiv JM_2M_1 \end{cases} \tag{17}$$

To satisfy the sliding condition, one proper choice of S_{sgabc} can be:

$$\{\ S_{sgabc} = E^+ S_{U\text{series}\alpha\beta}\ , \tag{18}$$

where E^+ is the Moore-Penrose pseudo-inverse matrix, which is specified as [34]:

$$\begin{cases} E^+ = E^T \left(EE^T\right)^{-1} = \begin{bmatrix} -1 & 0 \\ 0.5 & -0.866 \\ 0.5 & 0.866 \end{bmatrix} \end{cases} \tag{19}$$

The desired control signals are achieved by substituting Eq. (18) in Eq. (16). In the control rule of Eq. (16), changing the parameter has no effects in determining the sign of S_{sgabc}; thus, the proposed control algorithm is robust to the parameter changing as will be shown by simulations. Finally, the control scheme for SGSC is shown in Figure 3. $S_{wsg1}, S_{wsg2}, \cdots$, and S_{wsg6} are the transistors' ON-OFF gating signals, which can be obtained from Eq. (20) as follows:

$$\begin{cases} S_{wsg1} = 0.5(1 + U_{sgaN}/u_0); & S_{wsg4} = 1 - S_{wsg1}; \\ S_{wsg2} = 0.5(1 + U_{sgbN}/u_0); & S_{wsg5} = 1 - S_{wsg2}; \\ S_{wsg3} = 0.5(1 + U_{sgcN}/u_0); & S_{wsg6} = 1 - S_{wsg3}; \end{cases} \tag{20}$$

where $u_0 = Vdc/2$.

4. SMC of the GSC

As it is expressed in [26], the GSC must control the active and the reactive power of the grid-side by the

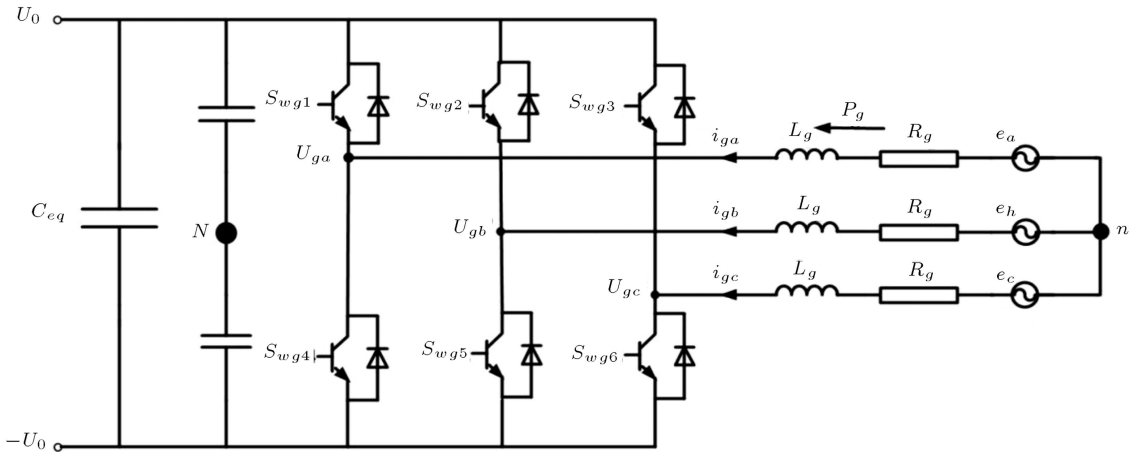

Figure 4. Structure of the GSC.

sliding-mode control and the DC-link voltage must be set to the reference value using a PI controller. This method is not robust against initial transient state and parameter variations (specially changing of the capacitor of the DC link), simultaneously. In addition, the fluctuations of the injected power to the network increase, which decrease the quality of the output power of the system. Therefore, in this paper, to solve these problems, the DC-link is controlled by the sliding-mode control method of [32], but with the difference that V_{dc}^2 is controlled (instead of $\frac{1}{V_{dc}}$), which has a more simple control algorithm.

Figure 4 shows the structure of the GSC. The equations of the GSC, which have been represented in [26], are expressed here as:

$$P_g = \frac{3}{2}(e_{\alpha n} i_{g\alpha} + e_{\beta n} i_{g\beta}), \tag{21}$$

$$Q_g = \frac{3}{2}(e_{\beta n} i_{g\alpha} - e_{\alpha n} i_{g\beta}), \tag{22}$$

$$e_{\alpha\beta n} = U_{g\alpha\beta n} + R_g i_{g\alpha\beta} + L_g \frac{di_{g\alpha\beta}}{dt}, \tag{23}$$

$$P_r = P_e - P_s, \tag{24}$$

$$P_e = \omega_r T_e, \tag{25}$$

$$\begin{cases} \begin{bmatrix} U_{g\alpha n} \\ U_{g\beta n} \end{bmatrix} = M_2 M_1 \begin{bmatrix} U_{gaN} \\ U_{gbN} \\ U_{gcN} \end{bmatrix} \\ \\ U_{g\alpha\beta n} \equiv M_2 M_1 U_{gN} \end{cases} \tag{26}$$

As shown in Figure 1, the common DC-link voltage can be obtained as follows:

$$\frac{1}{2} C_{eq} \frac{dV_{dc}^2}{dt} = P_g - P_{\text{series}} - P_r. \tag{27}$$

Defining $Z_2 = V_{dc}^2$ and substituting Eq. (24) in Eq. (27), we have:

$$\begin{cases} \frac{1}{2} C_{eq} \frac{dZ_2}{dt} = P_g - P_{\text{series}} - P_e + P_s \\ \\ \frac{1}{2} C_{eq} \frac{d^2 Z_2}{dt^2} = \dot{P}_g - \dot{P}_{\text{series}} - \dot{P}_e + \dot{P}_s \end{cases} \tag{28}$$

Taking the first time derivative of Q_g and the second order time derivative of Z_2, the relative degrees of the system will be 1 and 2, respectively. Therefore, similar to the method proposed in [32], the switching variables are defined as:

$$\begin{cases} S_{Z2} = \dot{e}_{z2} + 2c_{Z2} e_{Z2} + c_{Z2}^2 \int e_{Z2} dt \\ \\ S_{Qg} = e_{Qg} + c_{Qg} \int e_{Qg} dt \end{cases} \tag{29}$$

where e_{Z2} and e_{Qg} are the error of Z_2 and the error of the reactive power, respectively, which are:

$$\begin{cases} e_{Z2} = Z_2^* - Z_2 \\ \\ e_{Qg} = Q_g^* - Q_g \end{cases} \tag{30}$$

C_{Z2} and C_{Qg} in Eq (29) are positive control gains. The dynamics of the switching variables can be extracted by taking the derivatives of Eq. (29) as:

$$\begin{cases} \dot{S}_{Z2} = -\ddot{Z}_2 - 2c_{Z2} \dot{Z}_2 + c_{Z2}^2 (Z_2^* - Z_2) \\ \\ \dot{S}_{Qg} = \dot{Q}_g^* - \dot{Q}_g + c_{qg} (Q_g^* - Q_g) \end{cases} \tag{31}$$

Taking the derivations of Eqs. (5), (21), (22), and (25), the active, reactive, and electromagnetic powers instantaneous variations can be calculated as:

$$\begin{cases} \dot{P}_{\text{series}} = \dfrac{3}{2}\left(\dot{U}_{\text{series}\alpha} i_{s\alpha} + U_{\text{series}\alpha}\dot{i}_{s\alpha} + \dot{U}_{\text{series}\beta} i_{s\beta} \right. \\ \qquad\qquad \left. + U_{\text{series}\beta}\dot{i}_{s\beta}\right), \\ \dot{Q}_g = \dfrac{3}{2}\left(\dot{e}_{\beta n} i_{g\alpha} + e_{\beta n}\dot{i}_{g\alpha} - \dot{e}_{\alpha n} i_{g\beta} - e_{\alpha n}\dot{i}_{g\beta}\right) \\ \dot{P}_g = \dfrac{3}{2}\left(\dot{e}_{\alpha n} i_{g\alpha} + e_{\alpha n}\dot{i}_{g\alpha} + \dot{e}_{\beta n} i_{g\beta} + e_{\beta n}\dot{i}_{g\beta}\right) \\ \dot{P}_e = \dot{T}_e\omega_r + T_e\dot{\omega}_r \end{cases} \tag{32}$$

Substituting Eqs. (28) and (32) in Eq. (31) results in:

$$\begin{cases} \begin{bmatrix} \dot{S}_{Z2} \\ \dot{S}_{Qg} \end{bmatrix} = \begin{bmatrix} F_{Z2} \\ F_{Qg} \end{bmatrix} - \dfrac{3}{2L_g}\begin{bmatrix} \frac{-2}{C_{eq}} e_{\alpha n} & \frac{-2}{C_{eq}} e_{\beta n} \\ -e_{\beta n} & e_{\alpha n} \end{bmatrix}\begin{bmatrix} U_{g\alpha n} \\ U_{g\beta n} \end{bmatrix} \\ \dot{S}_{Z2Q_g} \equiv F_{Z2Qg} - BU_{g\alpha\beta n} \end{cases} \tag{33}$$

where:

$$\begin{cases} \dot{S}_{Z2Qg} = \begin{bmatrix} \dot{S}_{Z2} & \dot{S}_{Qg} \end{bmatrix}^T \\ F_{Z2Qg} = \begin{bmatrix} F_{Z2} & F_{Qg} \end{bmatrix}^T \\ B = \dfrac{3}{2L_g}\begin{bmatrix} \frac{-2}{C_{eq}} e_{\alpha n} & \frac{-2}{C_{eq}} e_{\beta n} \\ -e_{\beta n} & e_{\alpha n} \end{bmatrix} \end{cases} \tag{34}$$

and:

$$\begin{cases} F_{Z2} = g_1\left(\dot{e}_{\alpha n}, \dot{e}_{\beta n}, i_{g\alpha}, i_{g\beta}, \psi_{s\alpha}, \psi_{s\beta}, i_{r\alpha}, i_{r\beta}, \right. \\ \qquad \left. \omega_r, i_{s\alpha}, i_{s\beta}, v_{s\alpha}, v_{s\beta}, e_{Z2}\right) \\ F_{Qg} = g_2\left(\dot{e}_{g\alpha}, \dot{e}_{g\beta}, i_{g\alpha}, i_{g\beta}, e_{Qg}, \dot{Q}_g^*\right) \end{cases} \tag{35}$$

g_1 and g_2 are functions of the state variables. In accordance with Eq. (33), taking the first derivative of the switching variables, the control inputs will be achieved. Following the same plan presented in Section 3.2, the control inputs are:

$$U_{gN} = u_0 \text{sgn}(S_{gabc}), \tag{36}$$

where $S_{gabc} = \begin{bmatrix} S_{ga} & S_{gb} & S_{gc} \end{bmatrix}^T$.

Substituting Eqs. (26) and (36) in Eq. (33) results in:

$$\begin{cases} \dot{S}_{Z2Qg} = F_{Z2Qg} - BM_2M_1\begin{bmatrix} u_0\text{sgn}(S_{ga}) \\ u_0\text{sgn}(S_{gb}) \\ u_0\text{sgn}(S_{gc}) \end{bmatrix} \\ C \equiv BM_2M_1 \end{cases} \tag{37}$$

The sliding condition will be satisfied while S_{gabc} is selected as:

$$S_{gabc} = C^+ S_{PgQg}. \tag{38}$$

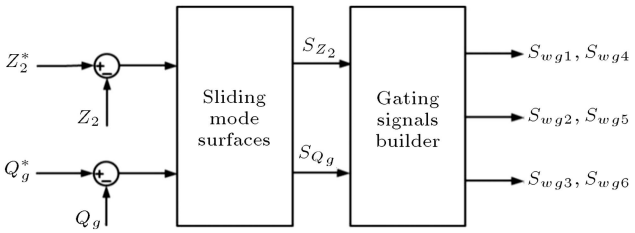

Figure 5. Control scheme of the grid-side power converter.

C^+ is the Moore-Penrose pseudo-inverse matrix, which is expressed as:

$$C^+ = C^T(CC^T)^{-1}$$

$$= \frac{2L_g}{3\left|e_{\alpha\beta n}\right|^2}\begin{bmatrix} \frac{-C_{eq}}{2} e_{\alpha n} & -e_{\beta n} \\ \frac{C_{eq}}{4}(e_{\alpha n} - \sqrt{3}e_{\beta n}) & \frac{1}{2}(e_{\beta n} + \sqrt{3}e_{\alpha n}) \\ \frac{C_{eq}}{4}(e_{\alpha n} + \sqrt{3}e_{\beta n}) & \frac{1}{2}(e_{\beta n} - \sqrt{3}e_{\alpha n}) \end{bmatrix}. \tag{39}$$

Substituting Eqs. (39) and (38) in Eq. (36), the desired control signals are achieved. The proposed control algorithm of GSC is robust against parameter variations. It is due to this fact that $2L_g/(3|e\alpha\beta n|^2)$ in C^+ has no effect on signs of S_{gabc}. The control scheme for GSC is shown in Figure 5.

Similar to Eq. (20), $S_{wg1}, S_{wg2}, \cdots$, and S_{wg6} are the transistors' ON-OFF gating signals, which can be expressed as:

$$\begin{cases} S_{wg1} = 0.5(1 + U_{gaN}/u_0); & S_{wg4} = 1 - S_{wg1}; \\ S_{wg2} = 0.5(1 + U_{gbN}/u_0); & S_{wg5} = 1 - S_{wg2}; \\ S_{wg3} = 0.5(1 + U_{gcN}/u_0); & S_{wg6} = 1 - S_{wg3}; \end{cases} \tag{40}$$

5. SMC of the RSC

The sliding-mode control of the RSC is similar to that of [26]. Based on the sliding-mode control, the RSC is used for control of the electromagnetic torque and for the stator reactive power. In the next section, the proposed method is simulated.

6. Control block diagram of DFIG with SGSC

The general block diagram for the control of a DFIG system with SGSC, which has been discussed in Sections 3 to 5, is shown in Figure 6.

7. Simulations of the DFIG system accompanied by SGSC

In order to test the proposed control strategy and further explain and evaluate it, simulations of a 2MW DFIG wind turbine and a 5 kW DFIG wind turbine with SGSC have been performed by using Matlab/Simulink with the time constant of 25 μs. Details

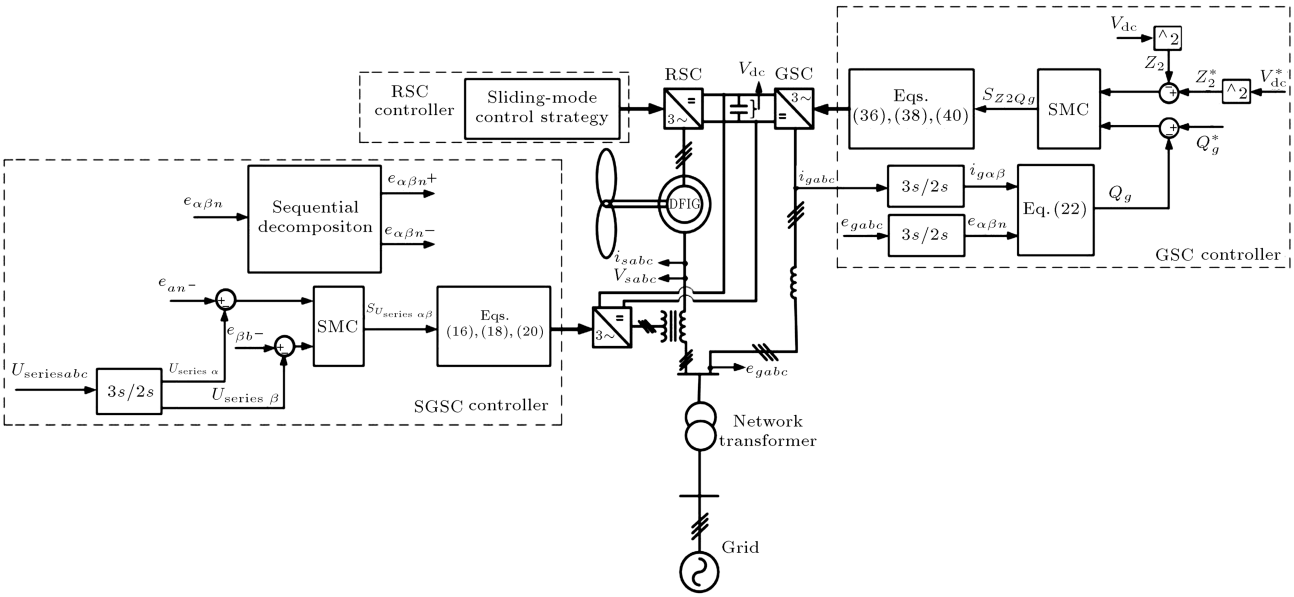

Figure 6. The control signals in the DFIG system with SGSC.

of the simulated 2 MW DFIG system with parameters were adapted from [32] and are given in Appendices A and D; moreover, practical parameters of 5 kW DFIG system with experimental parameters were adapted from [26,30] and are given in Appendices B and C. In accordance with [26], the set point of the stator active power is calculated from the rotor speed-optimal power curve and the set point of the stator reactive power is achieved with respect to the required 0.95 leading power factor.

The simulation results are divided into 4 parts and the corresponding results are compared with [26,32] to assess the proposed controller and evaluate its effectiveness.

Sections 7.1 and 7.2 show the desirable performance of the DFIG system accompanied by SGSC under unbalanced grid voltage conditions and Section 7.3 discusses the robustness of the proposed control strategy.

7.1. Simulation results of the 2MW DFIG system under unbalanced voltage conditions

As it is shown in Figure 7(a), at the initial time, a 15% drop in the voltage over the two phases effect unbalanced voltage source is considered. Also, after the second 5.5, the load is changed. Considering Figure 7(b)-(d), despite unbalanced voltage, the RSC (with the help of GSC) can control the electromagnetic torque as well as the reactive and the active power of the stator, as investigated in [26,32]. However, the oscillations with the frequency of 100 Hz still exist. Applying the SGSC by the proposed control algorithm, the amplitudes and ripples of these oscillations are considerably reduced. This in turn improves the operation of the DFIG system and the output power quality. The operation of RSC represented in [26] is similar to [32]. This implies that SMC of the RSC for both methods is the same.

In Figure 8, the DFIG structure of [32] is compared to that of [26]. It can be inferred from the figure that the DFIG structure of [32] has better performance than that of [26] in improving the quality of the active and the reactive output power. This is because of the proper control of GSC applied in [32]. But, as it is mentioned, the 100 Hz oscillations still exist, which reduce the output power quality. On the other hand, as it is seen from Figure 5, when the proposed control method is applied to the system, the oscillations in the DC-link voltage, the oscillations in the active and reactive power of the grid-side, and the oscillations in the reactive and active output power are reduced and the output power quality is considerably improved. Furthermore, the speed of dynamic response of the system is increased by using the proposed method.

The switching frequency spectrum of one of the switches is extracted and shown in Figure 8(d). It can be inferred from the figure that the frequencies which have large amplitudes are around 0-1500 Hz and higher order harmonics are negligible. Consequently, no filters are needed.

Also, for the three phase system, 15% drop in the voltage over the one phases effect unbalanced voltage source has been considered. The same analyses similar to the two phase unbalances have been done. The simulation results are depicted in Figures 9 and 10. By comparison between 2-phase and 1-phase unbalance simulation results, it can be inferred that the SMC method is independent of type disturbance.

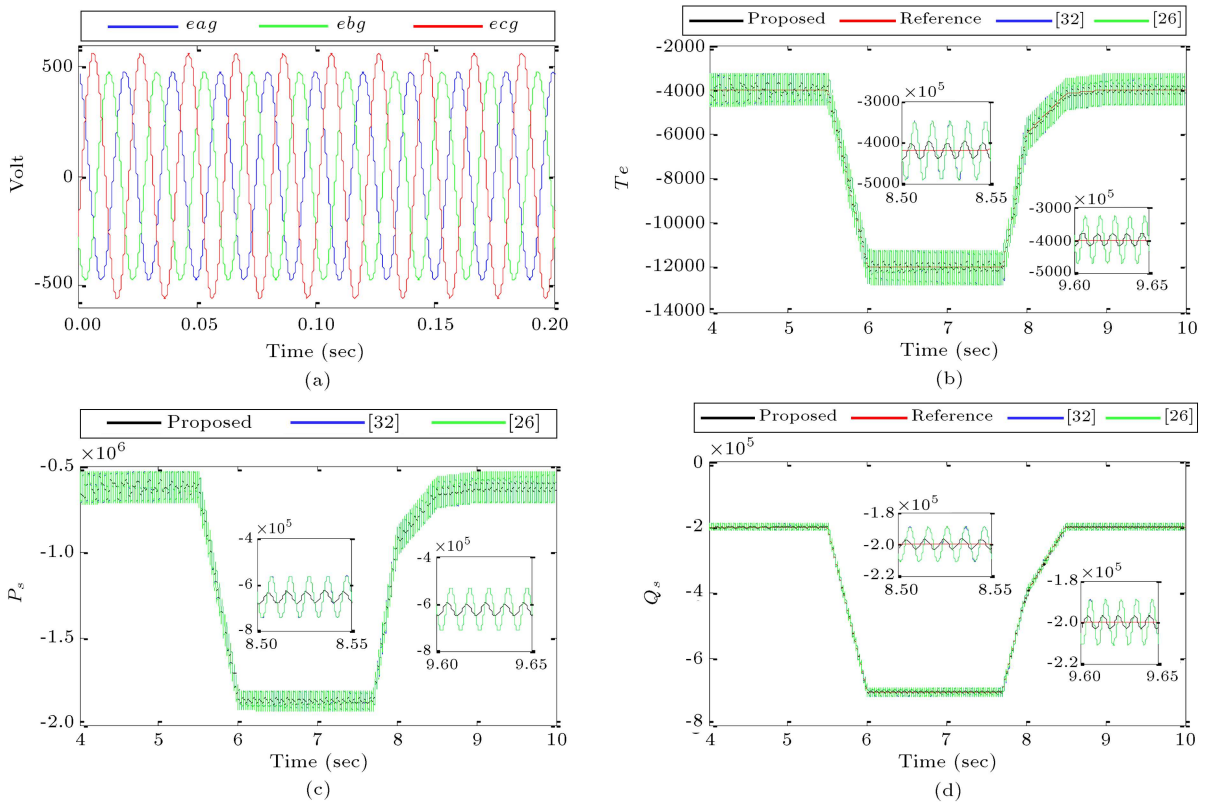

Figure 7. Simulation results under unbalanced voltage conditions (2-phase): (a) The grid voltage, (b) electro-magnetic torque, (c) stator active power, and (d) stator reactive power.

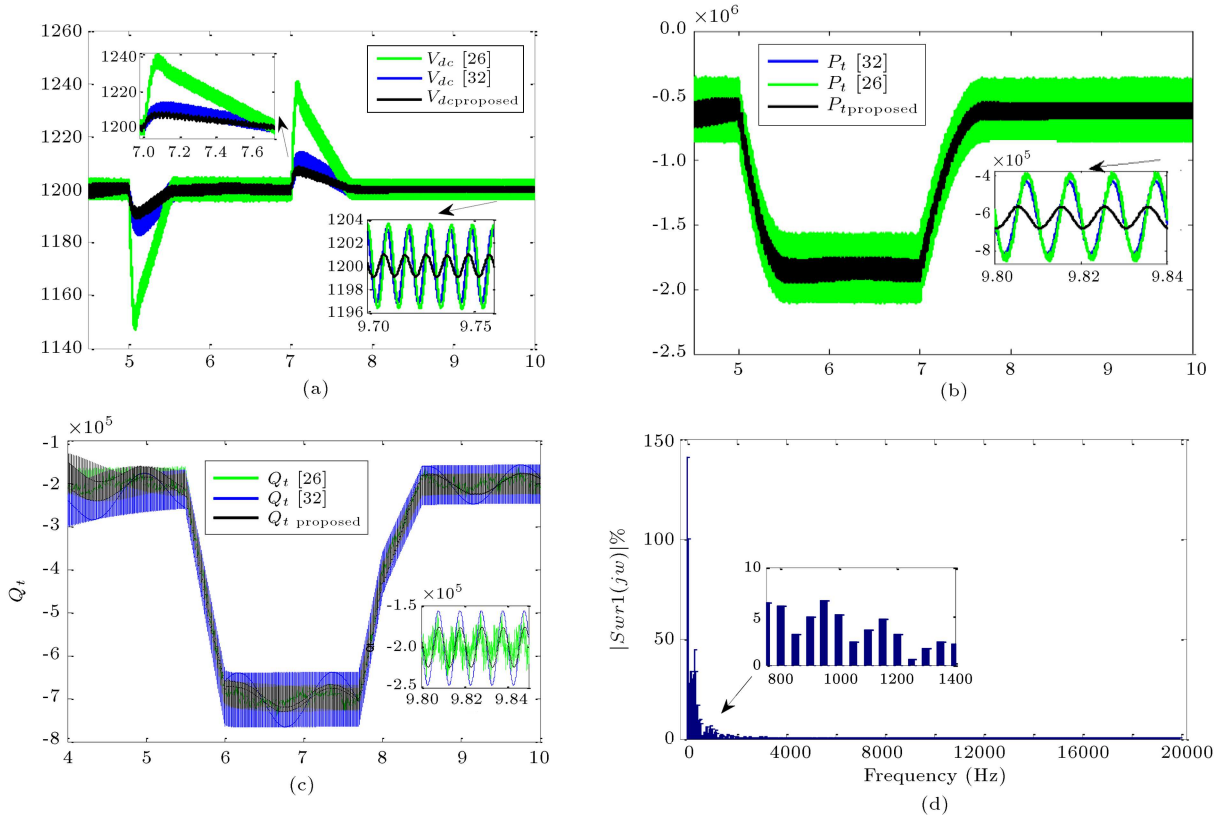

Figure 8. Simulation results under unbalanced voltage conditions (2-phase): (a) DC-link voltage, (b) total active power, (c) total reactive power, and (d) the frequency spectrum of gating signal S_{wr1}.

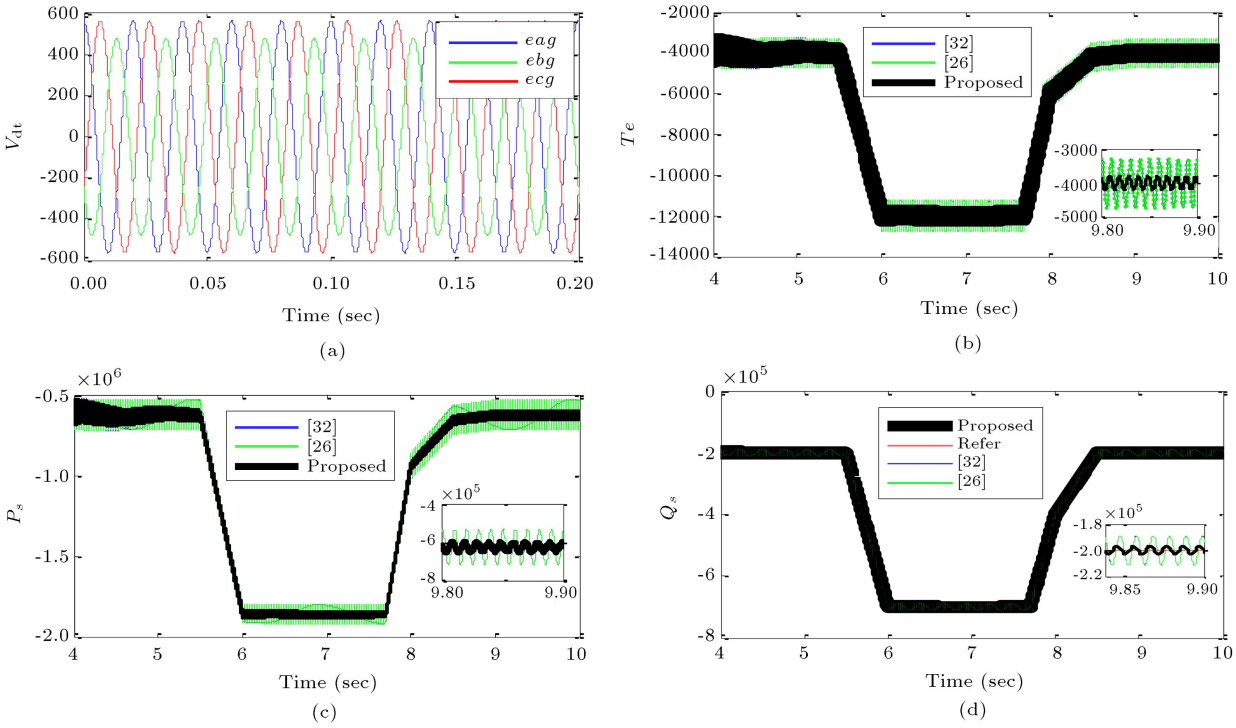

Figure 9. Simulation results under unbalanced voltage conditions (1-phase): (a) The grid voltage, (b) electro-magnetic torque, (c) stator active power, and (d) stator reactive power.

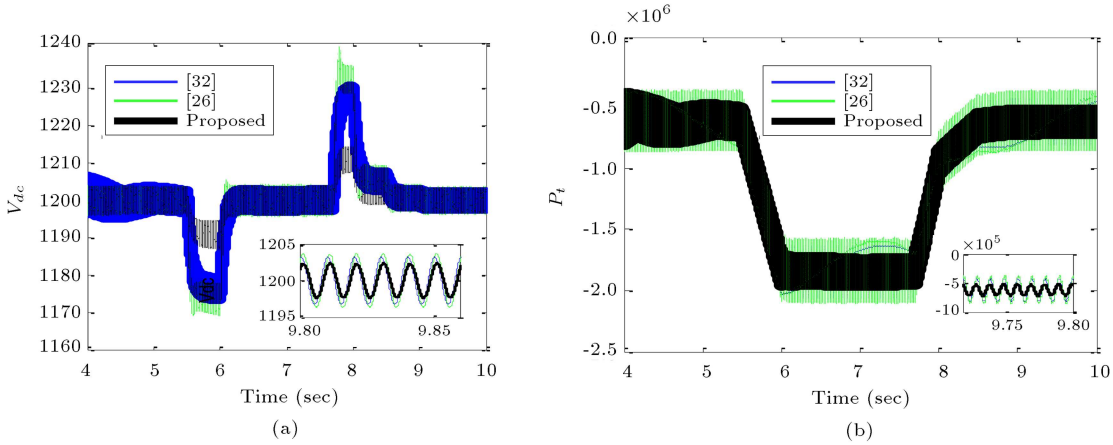

Figure 10. Simulation results under unbalanced voltage conditions (1-phase): (a) DC-link voltage, and (b) total active power.

7.2. Simulation results of the 5kW DFIG system under unbalanced voltage conditions

In this case, 10% voltage drop in 2 phases has been examined. The corresponding simulation results are depicted in Figure 11.

Figure 11 shows that by applying the proposed control method in this paper, the 100 HZ oscillations in active and reactive power, electromagnetic torque, and DC-Link voltage are considerably decreased. This fact improves the output power quality together with satisfactory performance of the DFIG system.

7.3. Simulation results for the robustness of the proposed method using the 2MW DFIG system

In order to find out the effects of parameter changing on the robustness of the proposed method, 2 cases are considered. In case I, DFIG parameters including stator and rotor resistances, and leakage inductance and magnetic inductance are changed by ±20%. In case II, converter parameters including capacitance, resistance, and leakage inductances are changed by –20%. The results were calculated for the 2 cases independently and they are depicted in Figures 12(a) and 12(b);

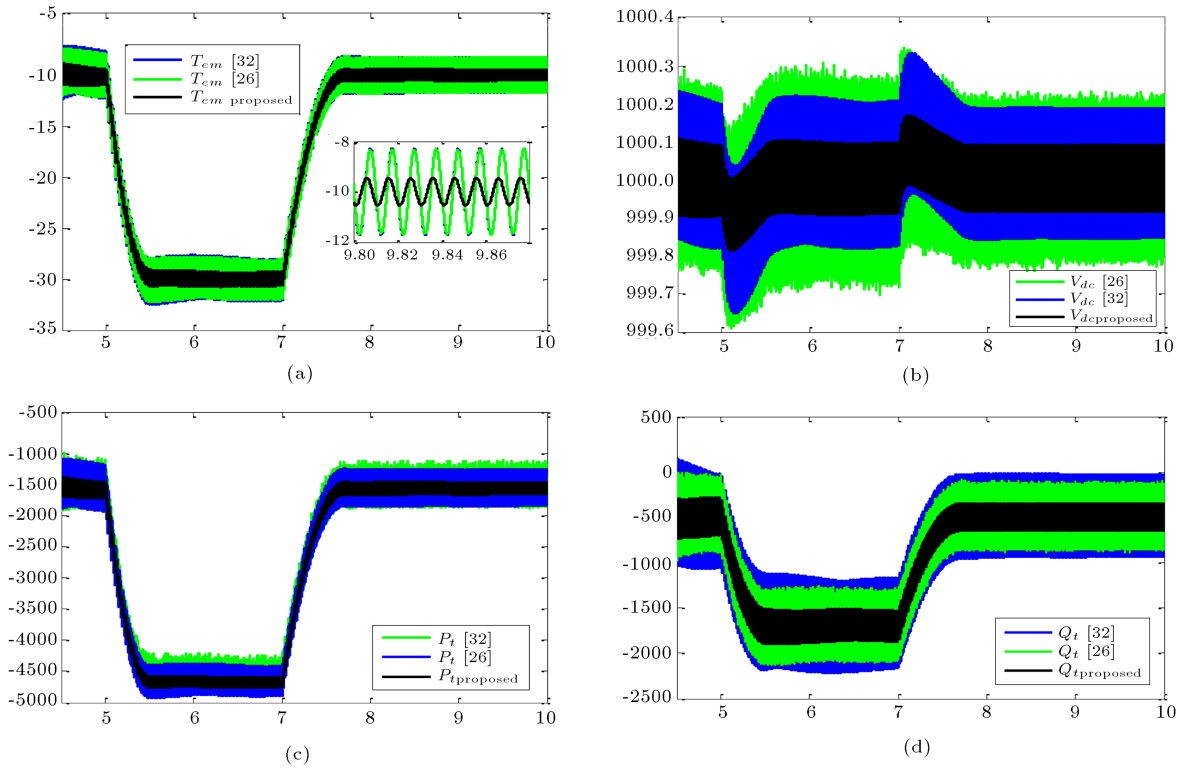

Figure 11. Simulation results under unbalanced voltage conditions (2-phase) with experimental system parameters: (a) electromagnetic torque, (b) DC-link voltage, (c) total active power, and (d) total reactive power.

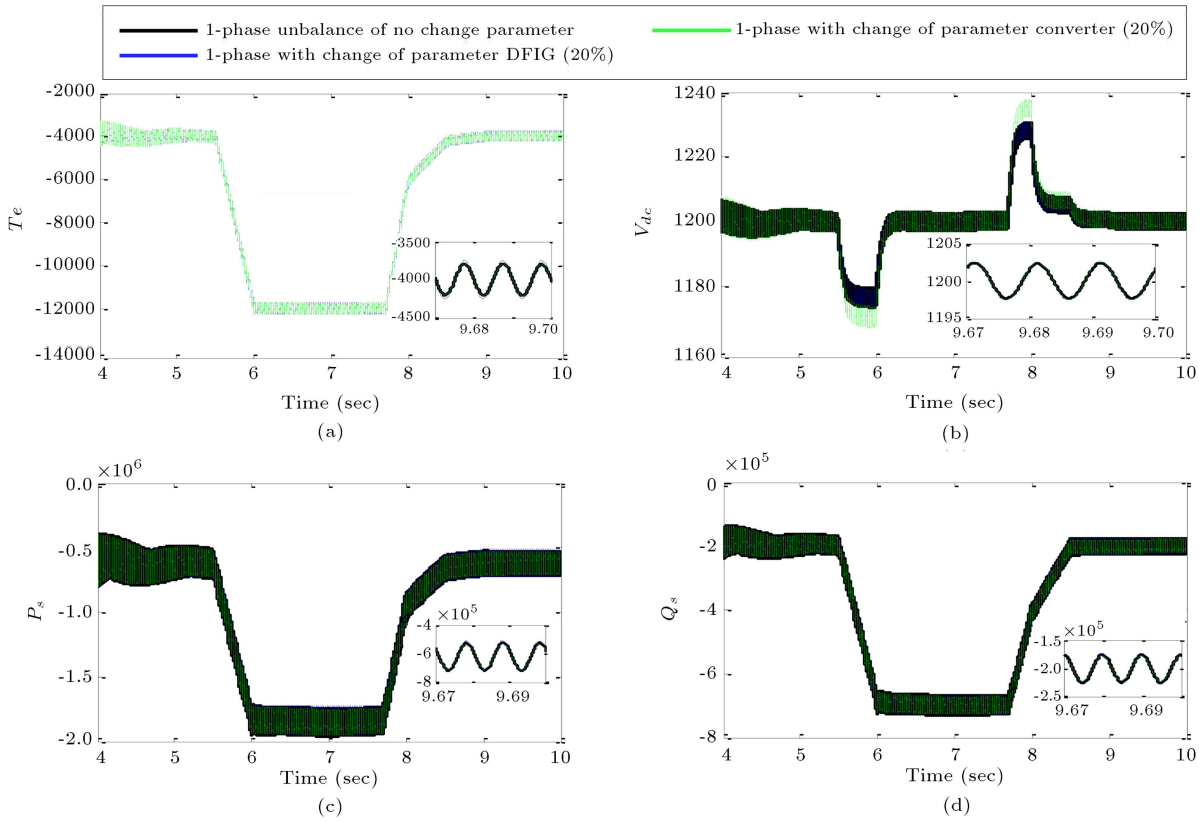

Figure 12(a). Simulation results under unbalanced voltage conditions (1-phase) with parameter variations: (a) Electromagnetic torque, (b) DC-link voltage, (c) total active power, and (d) total reactive power.

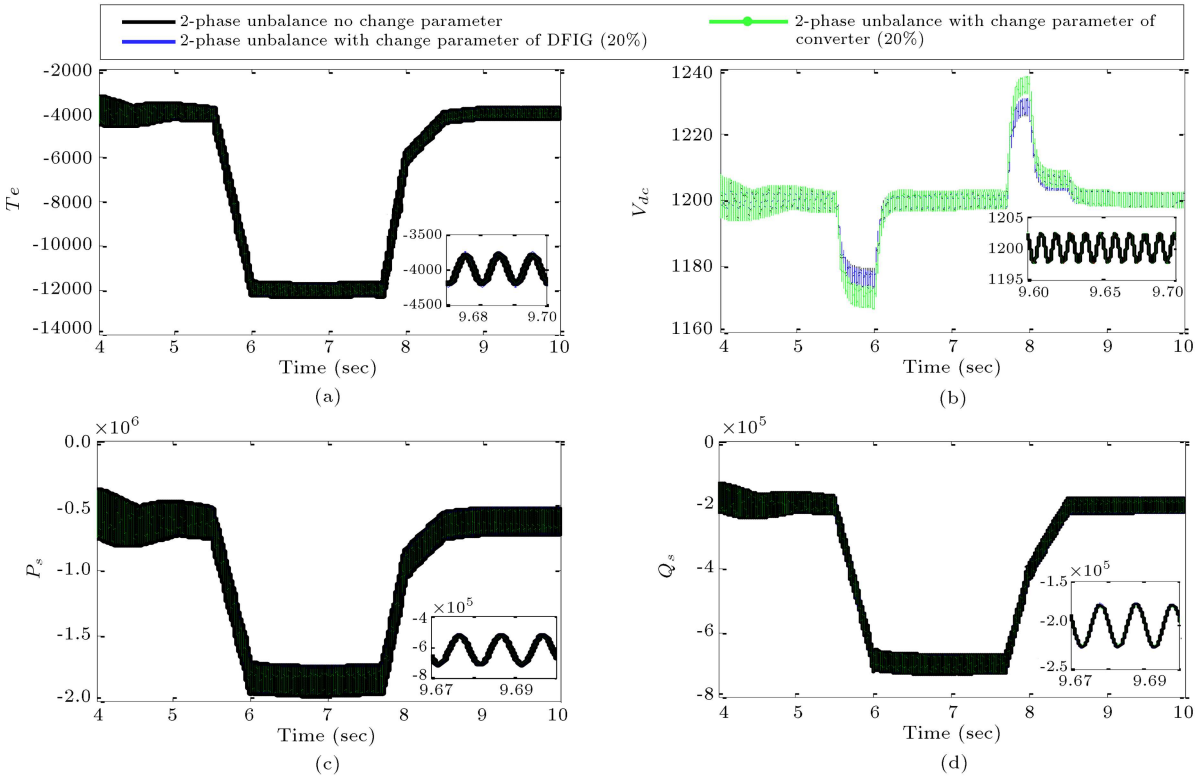

Figure 12(b). Simulation results under unbalanced voltage conditions (2-phase) with parameter variations: (a) Electromagnetic torque, (b) DC-link voltage, (c) total active power, and (d) total reactive power.

moreover, they are compared with the results of the system with nominal parameters. It can be inferred from the results that for the proposed method, the controlled variables (electromagnetic torque, active and reactive power, and DC-link voltage) are not changed practically with changing the parameters.

Also, the same process is done using the method presented in [32]. The simulation results are depicted and compared in Figures 13(a) to 13(d). Comparison between the results shows that changing the parameter by ±10% in the method presented in [32] would change the results noticeably in comparison with the SMC method.

Besides, compared with the simulation results of the previous section, the parameter variations of the system have negligible impact on the amplitude of the oscillations and performance of the control system. which is acceptable.

8. Conclusions

In this paper, the enhanced coordinated control of a DFIG-Based Wind-Power Generation System with SGSC under Unbalanced Grid Voltage Conditions including 1-phase and 2-phase unbalances was investigated. The proposed control scheme was based on SMC for the SGSC and GSC; it was simply implemented and it improved the operation of the DFIG system in both transient and steady states for unbalanced grid voltage. Additionally, the proposed method was able to cancel the oscillations of electromagnetic torque, and active and reactive power, which led to improvement of output power system.

The effect of parameter changing on the robustness of the proposed method was independently studied in two cases of DFIG parameter changing and converter parameter changing. The simulation results showed that the proposed method, compared with the existing methods in the literature, was significantly robust against parameter variations in the whole DFIG system and the connected network. Furthermore, the speed of dynamic response in the proposed method was highly improved compared to the methods presented in the literature. In addition, simulation results confirmed the proficiency of the proposed model with practical inputs and data.

Nomenclature

v_s, e_n	Stator and grid voltage vectors
U_{series}	Series injected voltage vector of series grid-side converter referred to as stator-side
i_s, i_r	Stator and rotor current vectors
i_g	Grid-side converter current vectors

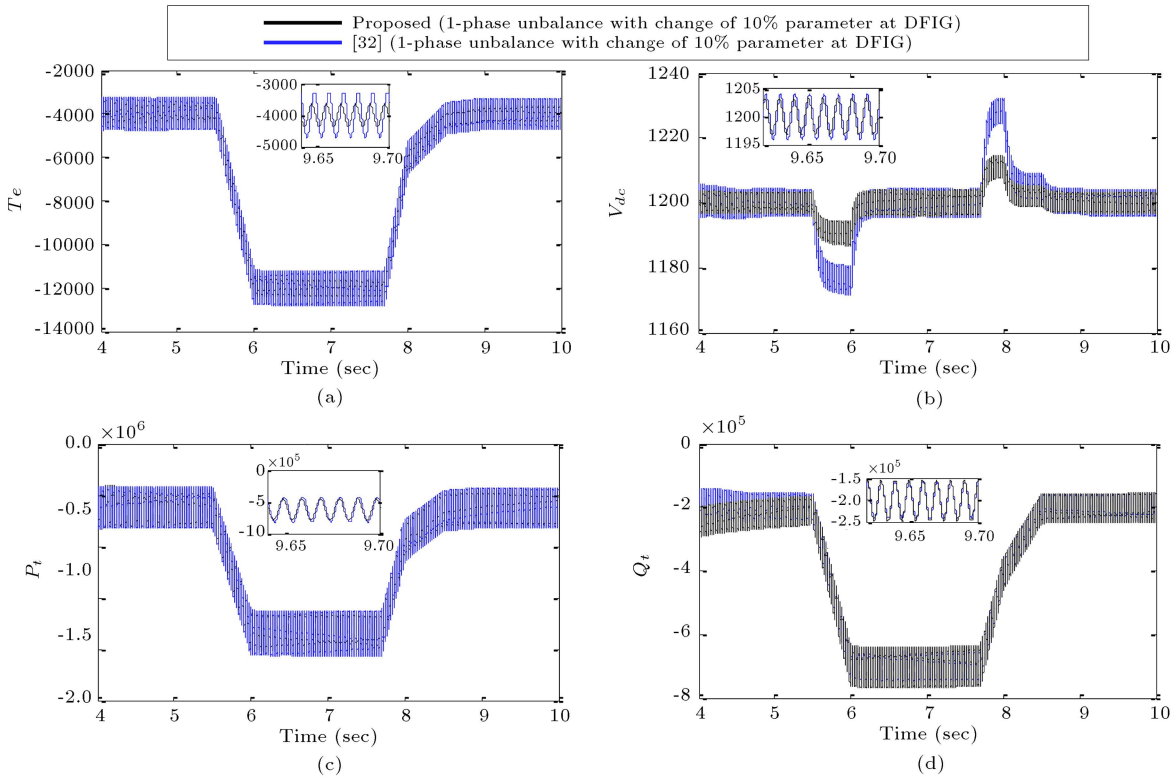

Figure 13(a). Simulation results under unbalanced voltage conditions (1-phase) with parameter variations at DFIG (comparing [32] with the proposed method): (a) Electromagnetic torque, (b) DC-link voltage, (c) total active power, and (d) total reactive power.

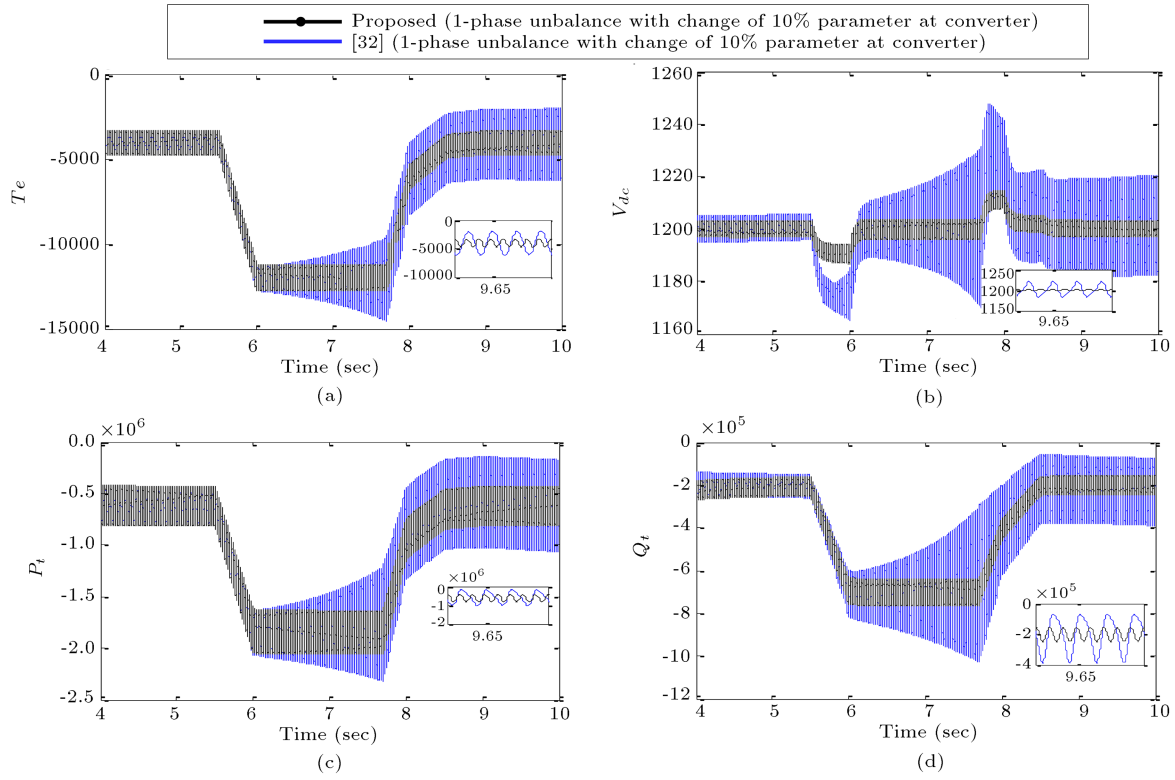

Figure 13(b). Simulation results under unbalanced voltage conditions (2-phase) with parameter variations at converter (comparing [32] with the proposed method: (a) Electromagnetic torque, (b) DC-link voltage, (c) total active power, and (d) total reactive power.

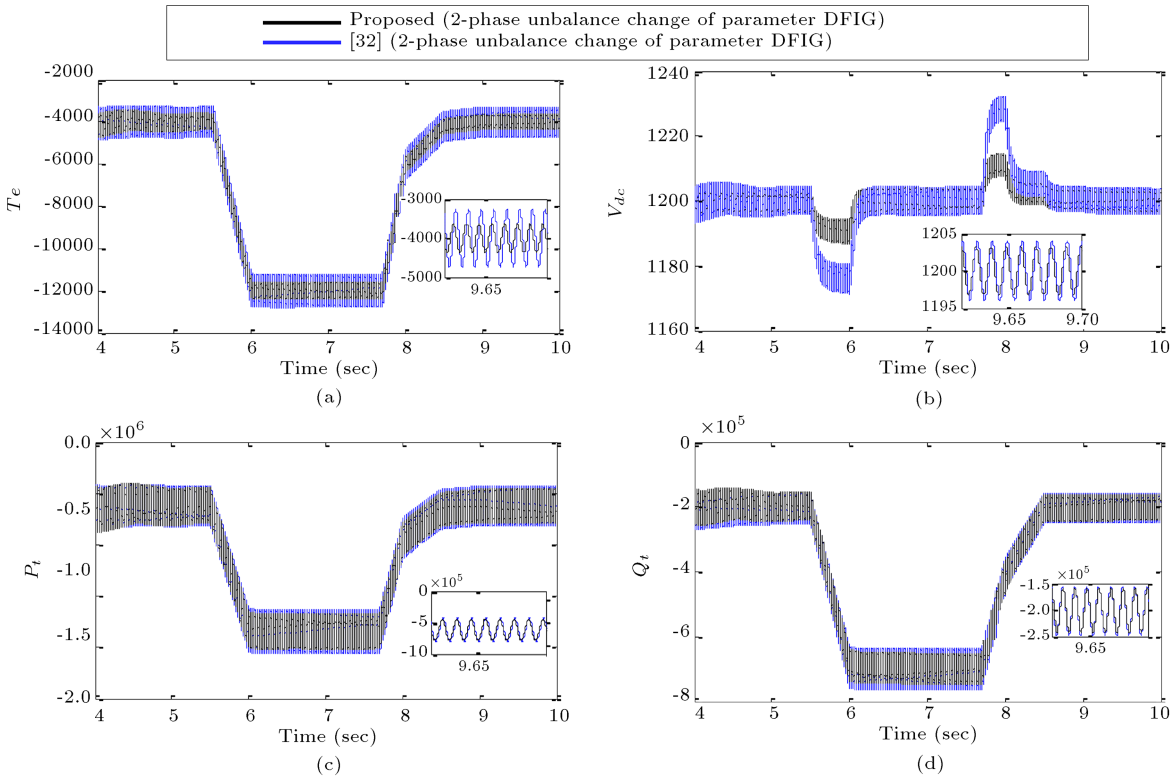

Figure 13(c). Simulation results under unbalanced voltage conditions (2-phase) with parameter variations at DFIG (comparing [32] with the proposed method): (a) Electromagnetic torque, (b) DC-link voltage, (c) total active power, and (d) total reactive power.

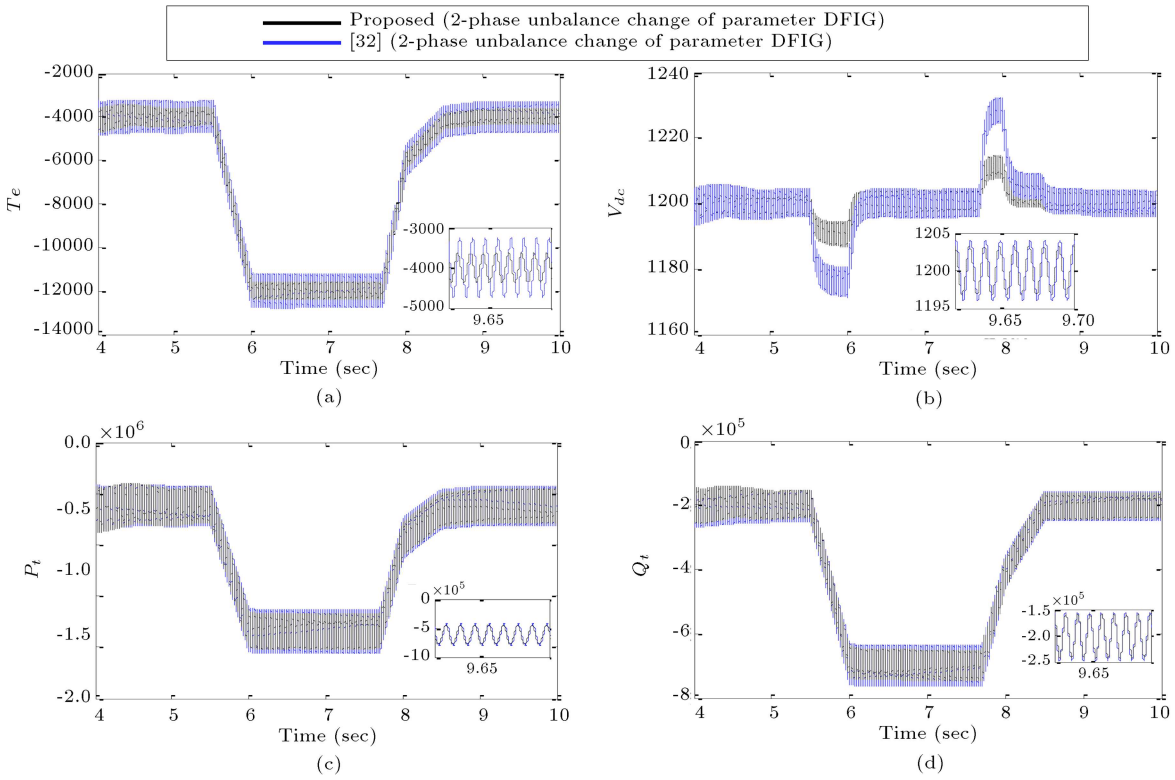

Figure 13(d). Simulation results under unbalanced voltage conditions (2-phase) with parameter variations at converter (comparing [32] with the proposed method): (a) electromagnetic torque, (b) DC-link voltage, (c) total active power, and (d) total reactive power.

L_g	Grid-side line inductance
L_m, L_r, L_s	Magnetizing, rotor, and stator inductances
$L_{\sigma s}, L_{\sigma r}$	Rotor and stator leakage inductances
P	Number of pole pairs
P_e	Electromagnetic power
P_s, Q_s	Stator output active and reactive power.
P_r, Q_r	Rotor output active and reactive power
P_g, Q_g	Grid-side converter output active and reactive power
$P_{\text{series}}, Q_{\text{series}}$	Active and reactive power through series grid-side converter
P_t, Q_t	Active and reactive power of the overall system
C_{eq}	DC-link equivalent capacitance
R_g	Grid-side line resistance
R_r, R_s	Rotor and stator resistances
V_{dc}	DC-link voltage
θ_r	Rotor electrical position
ω_r	Rotor electrical speed

References

1. Muljadi, E., Batan, T., Yildirim, D., and Butterfield, C.P. "Understanding the unbalanced-voltage problem in wind turbine generation", *Proc. Ind. Appl. Conference*, pp. 1359-1365, IEEE press (1999).
2. Brekken, T. and Mohan, N. "A novel doubly-fed induction wind generator control scheme for reactive power control and torque pulsation compensation under unbalanced grid voltage conditions", *PowerExpo. Spec. Conference*, pp. 760-766 (2003).
3. Piwko, R.N., Miller, N., Sanchez-Gasca, J., Yuan, X., Dai, R., and Lyons, J. "Integrating large wind farms into weak power grids with long transmission lines", *Proc. Power Electron. Motion Control Conf.*, pp. 1122-1128 (2006).
4. Kiani, M. and Lee, W.J. "Effects of voltage unbalance and system harmonics on the performance of doubly-fed induction wind generators", *IEEE Trans. Ind. Appl.*, pp. 562-568 (2010).
5. Muller, S., Deicke, M., and De Doncker, R.W. "Fed induction generator systems for wind turbines", *IEEE Ind. Appl. Mag.*, pp. 26-33, IEEE Press (2003).
6. Hu, J. and He, Y. "Dynamic modeling and robust current control of wind-turbine used DFIG during AC voltage dip", *J. Zhejiang Univ. Sci. A*, pp. 1757-64 (2006).
7. Pena, R., Clare, J.C., and Asher, G.M. "Doubly fed induction generator using back-to-back PWM converter and is application to variable-speed wind energy generation", *Proc. IEE B Electr. Power Appl.*, pp. 231-241 (1996).
8. Xu, L. and Cheng, W. "Torque and reactive power control of a doubly fed induction machine by position sensorless scheme", *IEEE Trans Ind.*, pp. 636-42 (1995).
9. Xu, L. and Wang, Y. "Dynamic modeling and control of DFIG based wind turbines under unbalanced network conditions", *IEEE Trans Power Syst.*, pp. 314-323, IEEE press (2003).
10. Xu, L. "Coordinated control of DFIG's rotor and grid side converters during network unbalance", *IEEE Trans Power Electron*, pp. 1041-104 (2008).
11. Hu, J. and He, Y. "DFIG wind generation systems operating with limited converter rating considered under unbalanced network conditions-analysis and control design", *Renewable Energy*, pp. 829-847 (2011).
12. Hu, J., He, Y., Xu, L., and Williams, B.W. "Improved control of DFIG systems during network unbalance using PI-R current regulators", *IEEE Trans Ind. Electron*, pp. 439-451 (2009).
13. Lai, Y.S. and Chen, J.H. "A new approach to direct torque control of induction motor drives for constant inverter switching frequency and torque ripple reduction", *IEEE Trans Energy Convers*, pp. 220-227 (2001).
14. Kang, J.K. and Sul, S.K. "New direct torque control of induction motor for minimum torque ripple and constant switching frequency", *IEEE Trans Ind.*, pp. 1076-1082, IEEE press (1999).
15. Datta, R. and Ranganathan, V.T. "Direct power control of grid-connected wound rotor induction machine without rotor position sensors", *IEEE Trans Power Electron*, pp. 390-399 (2001).
16. Xu, L. and Cartwright, P. "Direct active and reactive power control of DFIG for wind energy generation", *IEEE Trans Energy Convers*, pp. 750-758 (2006).
17. Abad, G., Rodriguez, M.A., and Poza, J. "Two-level VSC-based predictive torque control of the doubly fed induction machine with reduced torque and flux ripples at low constant switching frequency", *IEEE Trans Power Electron*, pp. 1050-1061 (2008).
18. Abad, G., Rodriguez, M.A., and Poza, J. "Two-level VSC-based predictive direct power control of the doubly fed induction machine with reduced power ripple at low constant switching frequency", *IEEE Trans Energy Convers*, pp. 570-580 (2008).
19. Kazemi, M.V., Yazdankhah, A.S., and Kojabadi, H.M. "Direct power control of DFIG based on discrete space vector modulation", *Renewable Energy*, pp. 1033-1042 (2010).

20. Zhi, D. and Xu, L. "Direct power control of DFIG with constant switching frequency and improved transient performance", *IEEE Trans Energy Convers*, pp. 110-118 (2007).

21. Hu, J., Nian, H., Hu, B., He, Y., and Zhu, Z.Q. "Direct active and reactive power regulation of DFIG using sliding-mode control approach", *IEEE Trans. Energy Convers*, pp. 1028-1039 (2010).

22. Susperregui, A., Tapia, G., Zubia, I., and Ostolaza, J.X. "Sliding-mode control of doubly-fed generator for optimum power curve tracking", *Electron. Lett.*, pp. 126-127 (2010).

23. Machmoum, M. and Poitiers, F. "Sliding-mode control of a variable speedwind energy conversion system with DFIG", *Proc. Ecol. Veh. Renewable Energies Int. Conf. Exhibit.*, pp. 1-7 (2009).

24. Zheng, X., Li, L., Xu, D., and Platts, J. "Sliding-mode MPPT control of variable speed wind power system", *Proc. Power Energy Eng. Conf.*, Wuhan, China, pp. 1-4 (2009).

25. Chen, S.Z., Cheung, N., Wong, K.C., and Wu, J. "Integral sliding-mode direct torque control of doubly-fed induction generators under unbalanced grid voltage", *IEEE Trans. Energy Convers.*, pp. 356-368 (2010).

26. Itsaso Martinez, M., Tapia, G., Susperregui, A., and Camblong, H. "Sliding-mode control for DFIG rotor- and grid-side converters under unbalanced and harmonically distorted grid voltage", *IEEE Trans. Energy Convers.*, pp. 328-338 (2012).

27. Shang, L. and Hu, J. "Sliding-mode-based direct power control of grid-connected wind-turbine-driven doubly fed induction generator under unbalanced grid voltage condition", *IEEE Trans. on Energy Conversion*, pp. 362-373 (2012).

28. Flannery, P.S. and Venkataramanan, G. "Unbalanced voltage sag ride-through of a doubly fed induction generator wind turbine with series grid-side converter", *IEEE Trans. Ind.*, pp. 1879-1887 (2009).

29. Liao, Y., Li, H., Yao, J., and Zhuang, K. "Operation and control of a grid connected DFIG-based wind turbine with series grid-side converter during network unbalance", *Electr. Power Syst. Res.*, pp. 228-236 (2011).

30. Yao, J., Li, H., Chen, Z., Xia, X., Chen, X., Li, Q., and Liao, Y. "Enhanced control of a DFIG-Based wind-power generation system with series grid-side converter under unbalanced grid volt-age conditions", *IEEE Trans. Power Electron.*, pp. 3167-3180 (2013).

31. Yao, J., Li, Q., Hen, Z., and Liu, A. "Coordinated control of a DFIG-based wind-power generation system with SGSC under distorted grid voltage conditions", *Energies*, pp. 2541-2561 (2013).

32. Abazari, S., Farajzadeh, S. and Taghipour, S. "Enhanced control of a DFIG-based system by sliding-mode control method during network disturbances", *Turkish Journal of Electrical Engineering & Computer Sciences*, **24**(5), pp. 3198-3212 (2016).

33. Utkin, V. "Sliding-mode control design principles and applications to electric drives", *IEEE Trans. Ind. Electronics*, pp. 23-36, IEEE press (1993).

34. Stephen, J., land, K., and Neumann, M., *Group Inverses of M-Matrices and their Application*, Chapman & Hall/CRC Applied Mathematics & Nonlinear Science (2012).

Appendix A

This section explains the subtitle mentioned in the equations.

Subscripts:

$\alpha\beta$	Stationary $\alpha\beta$-axis;
s, r	Stator and rotor;
g	Grid;
g,series	GSC and SGSC

Superscripts

$*$	Reference value

Appendix B

Simulation system parameters

A. Machine parameters:

- Ratings: $S_n = 2$ MW, $f_n = 50$ Hz, $U_n = 690$ V (Line-to-Line rms);
- Pole pairs: 2, winding connection (stator/rotor): Y/Y;
- Stator resistance: 2.6 mΩ;
- Stator leakage inductance: 77.306 μH;
- Rotor resistance: 2.9 mΩ;
- Rotor leakage inductance: 83.369 μH;
- Magnetizing inductance: 2.5 mH;
- Ns/Nr: 0.333;
- Lumped Inertia J: 30 kg.m^2.

B. Network transformer parameters:

- Ratings: $S_n = 2.5$ MW, $f_n = 50$ Hz;
- Primary windings: 20 kV-Yg;
- Secondary windings: 690 V-Δ;
- Short circuit impedance: $Z_T = 0.0098 + j0.09241$ pu.

C. Grid-side converter parameters:

- $L_g = 0.25$ mH, $R_g = 0.0$ Ω;
- DC-link equivalent capacitor: 38,000 μF;
- DC-link voltage reference value: 1200 V.

D. Series transformer parameters:

- Ratings: $S_n = 200$ kW, $f_n = 50$ Hz;
- Stator to SGSC side transformer turn ratio: 1:7;
- Sum of transformer and choke resistances: 0.006 pu;
- Sum of transformer and choke inductances: 0.03 pu.

Appendix C

Simulation system parameters

A. Machine parameters:

- Ratings: $S_n = 5$ kW, $f_n = 50$ Hz, $U_n = 690$ V (Line-to-Line rms);
- Pole pairs: 2, winding connection (stator/rotor): Y/Y;
- Stator resistance: 0.39 Ω;
- Stator leakage reactance: 6.53 Ω;
- Rotor resistance: 6.27 Ω;
- Rotor leakage reactance: 16.67 Ω;
- Magnetizing reactance: 296.99 Ω;
- Ns/Nr: 0.517.

B. GSC and RSC parameters:

- $L_g = 7$ mH, $R_g = 0.1$ Ω;
- DC-link equivalent capacitor: 2200 μF;
- DC-link voltage reference value: 1000 V.

C. Series transformer parameters:

- Ratings: $S_n = 2$ kVA, $f_n = 50$ Hz;
- Primary windings: 400 $V - Y$;
- Secondary windings: 400 $V - Y$.

Appendix D

Control parameters

- Proportional and integral gains: $K_P = 2800$ and $K_I = 100920$;
- Positive gains: $c_{te} = 1$, $c_{qs} = 1$, $c_{Z2} = 50$, $c_{qg} = 1$.

Biographies

Saeed Abazari received his BSc degree in Electrical Engineering from Isfahan University of Technology, Isfahan, Iran, in 1989; the MSc degree from Ferdowsi University, Mashhad, Iran, in 1992; and the PhD degree from Sharif University of Technology, Tehran, Iran, in 2002. Currently, he is a Professor in the Electrical Engineering Department at the University of Shahrekord, Shahrekord, Iran. His research interests are electric power distribution system, smart grid, power system operation and control, and FACTS controllers.

Sajad Farajzadeh Dehkordi was born in Shahrekord, Iran, on September 23, 1988. He received The BSc and the MSc degrees in Electrical Engineering and Power System Engineering from the University of Shahrekord, Iran, in 2010 and 2014, respectively. Afterwards, he joined the Electric Power Distribution Company of Chaharmahal and Bakhtiari Province, Iran. He is Lecturer in System Modeling and Control. His current research interests include wind power generation, control of electric drives based on vector, and direct torque control schemes, and electric power distribution system.